

# Self-Orienting Nanocubes for the Assembly of Plasmonic Nanojunctions

Bo Gao, Gaurav Arya, and Andrea R. Tao\*

## 1. Nanoparticle-Polymer Film Fabrication

**Nanocube synthesis.** Silver nanocubes were synthesized using a previously reported polyol reaction [1, 2]. The  $\text{AgNO}_3$  precursor solution was prepared by sonicating 0.20 g  $\text{AgNO}_3$  and 40  $\mu\text{L}$  of 0.043 M  $\text{CuCl}_2$  solution in 5 mL of 1,5-pentanediol until all the salt crystals were dissolved. 0.10 g PVP was dissolved in 5 mL pentanediol as precursor solution. The reaction solution was prepared by heating 20 mL pentanediol in a 100 mL glass round bottom flask under continuous stirring in an oil bath heated to 193°C. The  $\text{AgNO}_3$  and PVP precursor solutions were alternately injected into the hot pentanediol at a rate of 500  $\mu\text{L}/\text{min}$  and 320  $\mu\text{L}/30$  s, respectively. The injections were continued until the solution turned an opaque yellow color (after approximately 6 minutes). The nanocrystal solution was then characterized by UV-Vis spectroscopy using an Agilent Chemstation 8453. The as-made nanocrystal dispersions were diluted to a total volume of 50 mL using absolute ethanol and then centrifuged at 2500 rpm for 10 minutes (CL2, Thermo Scientific). The supernatant was further diluted to a 1:2 mixture of deionized water and ethanol to obtain a total dispersion volume of approximately 150 mL. This solution was then filtered through membranes with decreasing pores sizes (0.65 and 0.22  $\mu\text{m}$  PVDF hydrophilic Durapore filters, Millipore) to remove silver nanowires and large nanocrystals. The final solution was then centrifuged and redispersed at the desired concentration in ethanol.

**Film fabrication and annealing conditions.** Silicon and quartz substrates were further cleaned in a freshly prepared piranha solution of 70% (v) concentrated  $\text{H}_2\text{SO}_4$  and 30% (v)  $\text{H}_2\text{O}_2$ . The substrates were then treated with hexamethyldisilazane vapor at room temperature for 2hrs to obtain hydrophobic surfaces. Polystyrene was dissolved in a toluene solution at a concentration of 3 wt. % followed by

filtering through a membrane with a 0.02  $\mu\text{m}$  pore size. Polymer thin films were prepared by spin coating the filtered polymer solutions at 2000 rpm for 40s using a spin processor (WS-400A-6NPP/LITE) manufactured by Laurell Technologies Corp. Film thickness was measured by scratching the film and measuring the height profile by AFM. To prepare the composite film, nanocrystals were precipitated in a small amount of ethanol ( $\sim 100 \mu\text{l}$ ) before diluting with 1–2 ml  $\text{CHCl}_3$ . A glass petri dish was thoroughly rinsed with ethanol and DI water. The colloidal nanocrystal solution was then added dropwise to the air–water interface of the petri dish, leaving an isotropically distributed monolayer of NCs floating at the air–water interface. After the desired amount of colloidal solution was added, the film was allowed to equilibrate for about 15 min. Nanocrystal monolayers were then transferred onto the polystyrene films by dip-coating.

Nanoparticles are then embedded into the underlying polymer by thermal annealing ( $T > T_g$ ) or solvent vapor treatment at room temperature, which allows the polystyrene chains at the top of the film to rearrange around the sinking nanoparticle. Solvent annealing was carried out by exposing the polymer film to chloroform vapor in a closed vessel treatment at room temperature. Thermal annealing was carried out by heating the polymer films in ambient conditions at a temperature above the glass transition temperature of the matrix polymer, typically in the range of 95–120°C in an oven or on a hot plate. For the two-step annealing process used to convert EE-oriented nanocubes to FF-oriented nanocubes, the polymer film samples are first exposed to chloroform to form EE assemblies with a desired domain size before carrying out thermal annealing for 4 hours at 120°C.

**Sample characterization.** Nanoparticle assembly was characterized by scanning electron microscopy (SEM) using a FEI UHR Field Emission SEM equipped with a field emission cathode with a lateral resolution of approximately 2 nm. The acceleration voltage was chosen between 5 and 30 kV. Cross-sectional samples were prepared by sputtering a thin layer of Cr on top of the polymer surface followed by diamond scribing of the film support. Surface topologies of films were characterized with an atomic force microscope (Veeco, Multimode scope with a Nanoscope IV controller) operating in the tapping

mode. Roughness and line scan analyses were then used to characterize these surfaces. The raw data was processed with the Nanoscope IV software by a third-order plane fit and second order flattening. Silicon cantilevers were chosen (NSC, Mikromasch) with a resonance frequency around 300-400 kHz and a typical spring constant near 40 N/m. The plasmonic response of the nanoparticle assembly was characterized by measuring the optical transmission of the nanocomposite film deposited on a transparent quartz substrate.

## 2. Nanoparticle Chain Formation

Atomic force microscopy (AFM) topology and phase imaging indicate that upon thermal annealing ( $T \approx 100^\circ\text{C}$ ) for two hours, the nanoparticles are fully embedded in the PS film (Fig. S1). Particle migration to the PS/support interface is prevented by rendering the underlying solid support hydrophobic. For a film that has been thermal annealed for 120 minutes, AFM analysis indicates that the cubes are completely embedded into the polymer matrix but do not undergo lateral diffusion to form strings. (Fig. S1) After 24 hours of annealing, cross-sectional SEM images confirm that the nanoparticles assemble into strings but remain completely embedded in the matrix polymer near the PS/air interface (Fig. S2). The corresponding optical spectrum exhibits SP modes that correlate to isotropically distributed, isolated nanocubes. Upon further annealing, demixing of the nanoparticle/polymer blend occurs and nanocubes assemble into chains uniformly over extended areas ( $> 1 \text{ cm}^2$ ) limited only by the initial area of particle deposition.

Because spinodal decomposition is a non-equilibrium process, the rate and extent of nanoparticle assembly is strongly dependent on the diffusion kinetics of particles through the polymer matrix. Higher nanoparticle densities ( $> 20 \text{ cubes}/\mu\text{m}^2$ ) and lower polymer viscosities result in faster chain formation and growth. Meta-stable nanoparticle configurations are trapped by freezing the matrix polymer and halting particle mobility. The one-dimensional particle chains form in a convergent manner, first through the formation of small nanocube dimers and trimers that coalesce to form longer chain-like structures. These nanoparticle chains continue to merge, giving rise to branched and bifurcating chains. The resulting pattern is reminiscent of classical polymer-polymer spinodal decomposition, where elongation, branching, and bending of condensed periodic phases indicate competition between attractive and repulsive forces.

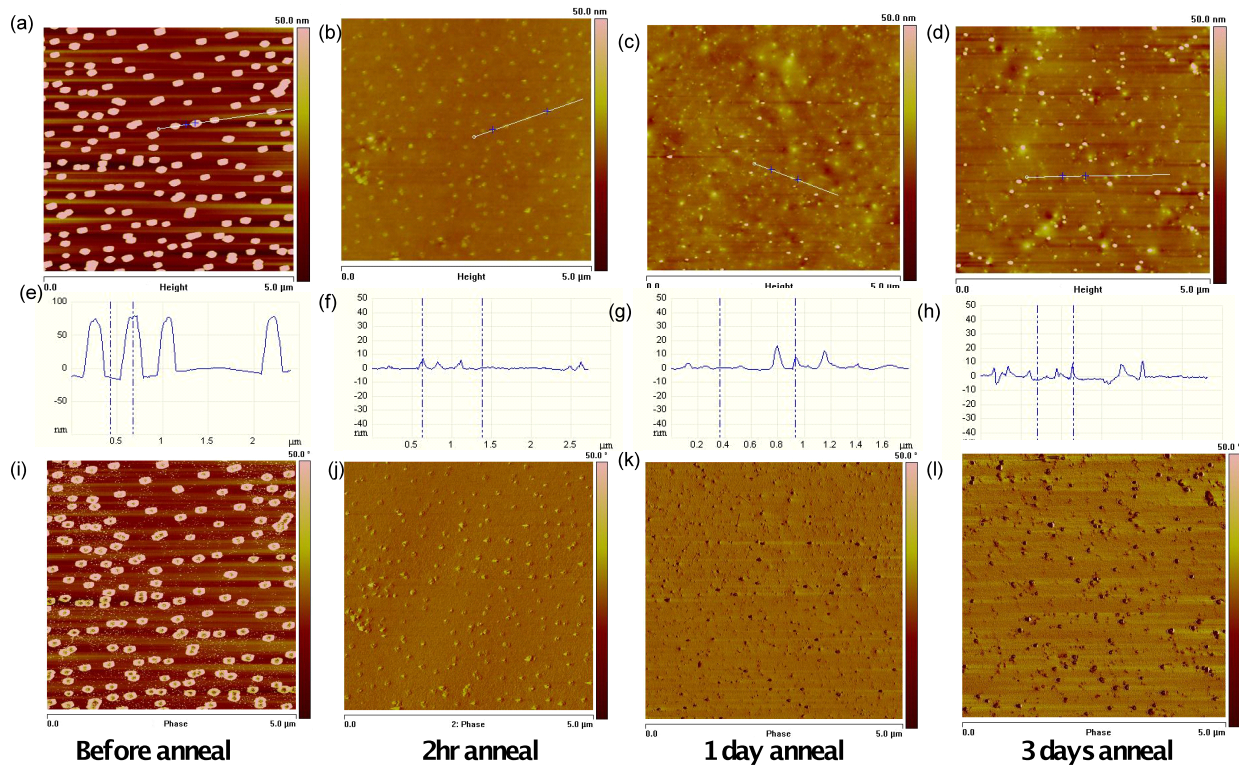


**Figure S1.** (a-d)  $5 \times 5 \mu\text{m}^2$  tapping mode AFM topographic images, (e-h) line scan profiles, and (i-l) phase images for silver nanocubes embedded into a PS film upon annealing at 120°C for 0, 2, 24, and 72 h.

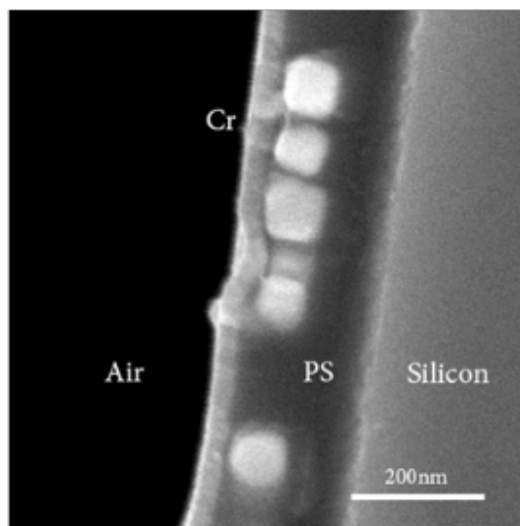


**Figure S2.** Cross-sectional SEM image of nanocubes embedded in a PS film after 24 h of annealing at 120°C.

### 3. Computational Methods

**Coarse-grained modeling of nanoparticles.** We aim to model the interactions between two polymer-grafted silver nanocubes of edge length 80 nm dispersed within a polymer matrix. However, since a fully atomistic treatment of the above system is computationally prohibitive due to the large system size and sluggish dynamics of the polymers, we choose to use a coarse-grained representation of the nanocubes. Also, many details of the experimental system remain unknown: for example, the surface grafting density of chains and their lengths and the molecular interactions between the grafted chains, the matrix polymer, and the silver surface are not known. To further alleviate computational effort, we examine smaller nanocubes of size  $l = 10$  nm. Results from these smaller nanocubes can then be extrapolated to the case of 80-nm nanocubes without much loss in accuracy through appropriate use of boundary conditions and scaling relations, as discussed later. This methodology allows us to capture the relevant qualitative trends for guiding our experimental efforts.

In our model, the silver nanocubes are treated as cubic lattices, each containing  $n_s = 15,625$  silver atoms. The cube thus represents a  $10\text{nm} \times 10\text{nm} \times 10\text{nm}$  section of the experimental  $80\text{nm} \times 80\text{nm} \times 80\text{nm}$  nanocube (Fig. S3). Accordingly, the two nanocubes in face-to-face (FF) orientation are grafted with polymer chains on the two sides facing each other while the nanocubes in the edge-to-edge (EE) orientation are grafted with chains on the four sides facing each other. Each of these “facing” surfaces is grafted with 4 polymer chains, yielding a grafting density of  $0.04$  chains/ $\text{nm}^2$  and a total of  $n_c = 8$  and  $16$  chains for the FF and EE configurations, respectively. The grafted chains are treated as coarse-grained bead-chains [3,4] comprising of  $L = 4$  to  $16$  beads, depending on the chain lengths being studied. Our model does not explicitly include matrix polymer chains. Instead, it implicitly accounts for the interactions between the matrix chains and the grafted chains through the use of “effective” interactions between the grafted chains, in similar spirit as the Flory-Huggins  $\chi$  parameter. We employ periodic boundary conditions (PBCs) to mimic both the remaining portion of the nanocube and the polymer chains

attached to it, as illustrated in Fig. S3. Thus, for the FF orientation, we employ PBCs in the two directions along the facing surface (along  $y$  and  $z$  axes in Fig. S3A), while for the EE orientation, we employ PBCs only in the direction along the facing edges (along  $z$  axis in Fig. S3B).

The two silver nanocubes interact with each other through van der Waals interactions, which is treated in our model using a Lennard-Jones (LJ) potential summed over all pairs of atoms  $i$  and  $j$  interacting across the two cubes. The total van der Waals energy  $U_{ss}$  is then given by

$$U_{ss} = \sum_{i=1}^{n_s} \sum_{j=1}^{n_s} 4\epsilon_{ss} \left[ \left( \frac{\sigma_{ss}}{r_{ij}} \right)^{12} - \left( \frac{\sigma_{ss}}{r_{ij}} \right)^6 \right] \quad \dots(1)$$

where  $r_{ij}$  is the distance between the interacting pairs of atoms,  $\sigma_{ss} = 0.256$  nm is the LJ size parameter for silver atoms and  $\epsilon_{ss}$  is the LJ energy parameter between silver atoms. Since, this parameter is not known apriori, we have derived it from the Hamaker constant  $A_{ss}$  of silver using the relation [5]

$$\epsilon_{ss} \approx \frac{A_{11}\sigma_{ss}^6}{4\pi^2\rho^2} \quad \dots(2)$$

where  $\rho$  is number density of silver atoms in the fcc lattice. Using a value of  $A_{11} = 3.9 \times 10^{-19}$  J for the Hamaker constant [6] and standard density of silver, we obtain a value of  $\epsilon_{ss} = 1.23$  kcal/mol.

The grafted polymer chains are treated as bead-chains with a bonded force field composed of harmonic stretching and bending terms. The chains are attached via a harmonic spring to the cube surface. The attachment positions, denoted  $\mathbf{r}_{i0}$  for chain  $i$ , are placed periodically on the cube surface 5 nm apart from each other. The total intramolecular energy of all chains is given by

$$U_{intra} = \sum_{i=1}^{n_c} \left( k_s |\mathbf{r}_{i1} - \mathbf{r}_{i0}|^2 + \sum_{j=1}^{L-1} k_s (l_{ij} - l_0)^2 + \sum_{j=1}^{L-2} k_\theta (\theta_{ij} - \theta_0)^2 \right) \quad \dots(3)$$

where  $i$  is the index of the chain,  $\mathbf{r}_{i1}$  is the position of the first bead attached to the surface,  $k_s$  and  $k_\theta$  are the stretching and bending constants, respectively,  $l_{ij}$  is the bond length between beads  $j$  and  $j+1$  of chain  $i$ ,  $\theta_j$  is the bonding angle between beads  $j, j+1$ , and  $j+2$  of chain  $i$ , and  $l_0$  and  $\theta_0$  are the equilibrium bond lengths and angles. The equilibrium bond lengths are fixed to  $l_0 = 1$  nm and bond angles are fixed to  $180^\circ$ . A sufficiently small  $k_\theta = 0.1$  kcal/mol/rad<sup>2</sup> ensures that the polymer remains flexible over length scales

larger than the bond length and a large  $k_s = 10$  kcal/mol/nm<sup>2</sup> ensures that the bond lengths remain fairly rigid.

The grafted polymer chains interact with each other through excluded volume interactions, treated using the Lennard-Jones potential. The total polymer-polymer interaction energy  $U_{pp}$  is given by

$$U_{pp} = \sum_{i=1}^{n_c} \sum_{k=1}^L \sum_{j=i+1}^{n_c} \sum_{l=1}^L 4\epsilon_{pp} \left[ \left( \frac{\sigma_{pp}}{r_{ikjl}} \right)^{12} - \left( \frac{\sigma_{pp}}{r_{ikjl}} \right)^6 \right] \quad \dots(4)$$

$$+ \sum_{i=1}^{n_c} \sum_{k=1}^{L-3} \sum_{l=k+3}^L 4\epsilon_{pp} \left[ \left( \frac{\sigma_{pp}}{r_{ilk}} \right)^{12} - \left( \frac{\sigma_{pp}}{r_{ilk}} \right)^6 \right] \quad \dots(5)$$

where the sum  $i$  and  $j$  runs over polymer chains and  $k$  and  $l$  over beads within each chain. The first term represents interactions between beads from separate chains and the second term represents interactions between beads of the same chain at least two beads apart from each other. Also,  $\sigma_{pp} = 1$  nm represents the size of each polymer bead, signifying a collection of several monomers, and  $\epsilon_{pp}$  represents the effective energy parameter between the grafted polymer (accounts for polymer-matrix and matrix-matrix interactions). Our calculations show that as long as  $\epsilon_{pp} < k_B T$ , it only minimally affects the interactions between the nanoparticles. Thus, we set  $\epsilon_{pp}$  to 0.1 kcal/mol, which results in a slight attraction between the chains but more importantly accounts for the excluded volume effect between the chains.

Finally, the interactions between the polymer chains and the nanocubes is also treated using the Lennard-Jones potential,  $U_{ps}$ , and is given by

$$U_{ps} = \sum_{i=1}^{n_c} \sum_{j=1}^{2n_s} 4\epsilon_{ps} \left[ \left( \frac{\sigma_{ps}}{r_{ij}} \right)^{12} - \left( \frac{\sigma_{ps}}{r_{ij}} \right)^6 \right] \quad \dots(6)$$

where indices  $i$  and  $j$  runs over chain beads and the atoms of the two nanocubes, respectively. Also, the LJ size parameter for this interaction  $\sigma_{ps}$  is taken to be 0.632 nm (the average of  $\epsilon_{pp}$  and  $\epsilon_{ss}$ ) while the LJ energy parameter  $\epsilon_{ps}$  is varied between 0.02 and 0.08 kcal/mol, which lead to per bead adsorption energies in the range  $\sim 0.3$ – $1.2$  kcal/mol (compare to  $k_B T \equiv 0.6$  kcal/mol).

The total interaction energy between the two polymer-grafted nanocubes is then given by the sum of the three van der Waals/excluded volume and intramolecular energy terms

$$U_{tot} = U_{ss} + U_{pp} + U_{ps} + U_{intra} \quad \dots(7)$$

The above force field is employed in our Monte Carlo simulation to compute the average potential energy of our two-nanocube system at varying separation distances. This force field is also used to compute the average force experienced by one of the particles, which is then used to compute the “effective” free energy of interaction between the particles, i.e., the potential of mean force.

**Potential of mean force calculations.** To determine the most favorable relative orientation of polymer-grafted nanocubes assembled as dimers, we compute the potential of mean force (PMF) between two polymer-grafted Silver nanocubes. We compute the PMF  $W(d, \theta)$  as a function of nanocube center-to-center distance  $d$  and relative orientations  $\theta$  (angle subtended by the interacting nanocube faces). We consider two main orientations: FF with  $\theta = 0$  and EE with  $\theta = \pi/2$ , as shown in Fig. S3. The PMF is computed by integrating the average force  $\langle F(d, \theta) \rangle$  experienced by the nanocube along the center-to-center line:[7]

$$W(d, \theta) = - \int_{\infty}^d \langle F(\xi, \theta) \rangle d\xi \quad \dots(8)$$

The average force is computed as the ensemble average over all configurational degrees of freedom of the grafted chains  $\Omega$ [3,4]

$$\langle F(d, \theta) \rangle = \frac{\int \dots \int - \left( \frac{\partial U_{tot}(d, \theta, \Omega)}{\partial d} \right) \exp(-U_{tot}(d, \theta, \Omega)/k_B T) d\Omega}{\int \dots \int \exp(-U_{tot}(d, \theta, \Omega)/k_B T) d\Omega} \quad \dots(9)$$

where  $U_{tot}$  is the total energy computed using Eqs. (1-7). To compute the right hand side of Eq. (9), we generate Boltzmann distributed configurations of the two colloids at fixed relative orientation for each separation distance  $d$  using Monte Carlo (MC) simulations at a fixed temperature of 300 K. The MC simulations comprise of “chain regrowth” moves, where the polymer chain is randomly chosen and regrown from scratch using the configurational bias MC approach.[8-10] The regrown chain is then accepted with the Rosenbluth acceptance criterion:

$$p_{acc} = \min \left[ 1, \frac{W_{new}}{W_{old}} \right] \quad \dots(10)$$

where  $W_{old}$  and  $W_{new}$  are the Rosenbluth weights of the original and regrown chain, respectively.

We can also compute the energetic contribution  $\Delta U(d,\theta) \equiv U(d,\theta) - U(\infty,\theta)$  to this PMF or free energy, where  $U(d,\theta)$  is the average energy at separation distance  $d$  and  $U(\infty,\theta)$  is the average energy at an infinite distance or a sufficiently large distance where the nanoparticles do not interact. The former is determined from the same MC simulation as

$$\mathcal{U}(d,\theta) \equiv \langle U_{tot}(d,\theta) \rangle = \frac{\int \cdots \int U_{tot}(d,\theta,\mathbf{\Omega}) \exp(-U_{tot}(d,\theta,\mathbf{\Omega})/k_B T) d\mathbf{\Omega}}{\int \cdots \int \exp(-U_{tot}(d,\theta,\mathbf{\Omega})/k_B T) d\mathbf{\Omega}} \quad \dots(11)$$

while the latter is taken to be equal to twice the energy of isolated nanoparticles.

Finally, the entropic contribution  $T\Delta S(d,\theta)$  to the PMF is computed from the standard thermodynamic relationship

$$T\Delta S(d,\theta) = \Delta \mathcal{U}(d,\theta) - \mathcal{W}(d,\theta) \quad \dots(12)$$

The above approach thus provides a convenient route towards obtaining the energetic and entropic driving forces for the observed interactions between polymer-grafted nanocubes.

**Extrapolation to large nanocubes.** The  $\Delta U(d,\theta)$ ,  $T\Delta S(d,\theta)$ , and  $W(d,\theta)$  computed through the above method relate to the two 10-nm sized nanocubes being simulated. The three quantities can be extrapolated to the larger nanocubes explored experimentally from our observations that  $\Delta U(d,\theta)$ ,  $T\Delta S(d,\theta)$ , and  $W(d,\theta)$  all scale as  $l^2$  in the case of FF orientation ( $\theta = 0$ ) and as  $l$  in the case of EE orientation ( $\theta = \pi/2$ ), where  $l$  is the edge length of the nanocube. Accordingly,  $\Delta U(d,\theta)$ ,  $T\Delta S(d,\theta)$ , and  $W(d,\theta)$  computed from our simulations need to be multiplied by factors of  $8 \times 8$  (FF orientation) and 8 (EE orientation) to extrapolate them to the case of 80-nm nanocubes. Below we provide an explanation for the above scalings.

We first consider the FF-oriented nanocubes. The total energy change  $\Delta U(d,\theta)$  for approaching nanocubes has three contributions: (i)  $\Delta U_{ss}$ , the change in vdW attraction; (ii)  $\Delta U_{pp}$ , the change in the interactions between grafted polymers; and (iii)  $\Delta U_{ps}$ , the change in the interactions between the polymer and the nanocubes. Several studies have shown that the vdW interactions between two face-to-face cuboids [11] and between two half-spaces [12] scale as  $l^2$  at short separation distances. We have

confirmed the  $l^2$  scaling by computing  $\Delta U_{ss}$  [via Eq. (1)] for nanocubes of varying sizes  $l$  in the range 2–12 nm separated by small gaps ( $d - l$ ) = 0.1–10 nm relevant to self-assembly (Fig. S6a). The other two energy terms,  $\Delta U_{pp}$  and  $\Delta U_{pp}$ , should scale with the number of grafted chains interacting between the two proximal nanocubes, which is proportional to the surface area  $l^2$  (excluding boundary effects) of the opposing nanocube faces. Similarly, the entropic loss  $-T\Delta S$  incurred by the compressed grafted chains in between the two nanocubes is also expected to be proportional to the number of compressed chains, which also scales as the surface area  $l^2$ . Thus, the total change in the energy and entropy as well as the PMF  $W(d,\theta)$  are expected to scale as  $l^2$  for FF-orientated nanocubes.

We next examine the EE-oriented nanocubes. Previous calculations [11] suggest that  $\Delta E_{vdW}$  exhibits a scaling of  $l^1$  for EE oriented cuboids separated by small distances. The above  $l^1$  scaling has been verified for our nanocubes of sizes  $l = 2$ –12 nm for gaps ( $d - \sqrt{2}l$ ) in the range 0.1–10 nm (Fig. S6b). The remaining energy terms,  $\Delta U_{ps}$  and  $\Delta U_{pp}$ , and the entropic loss ( $-T\Delta S$ ) all scale with the number of grafted chains involved in inter-particle interactions. However, we note here that only chains close to the two facing edges of the nanocubes are involved in inter-particle interactions, while the remaining chains are too short to reach the opposite nanocube surface and its grafted chains. If the mean height of the grafted chains from the surface of the nanocubes is  $\delta$ , then it can be shown that only chains within a distance  $\delta$  from the nanocube edge (assuming  $\delta < l$ ) can mediate interactions with the apposing nanocubes. Thus, the number of interacting chains is proportional to the surface area  $\delta \times l$  in the EE orientation, rather than the  $l^2$  observed in the FF orientation. Thus, the total change in the energy and entropy as well as  $W(d,\theta)$  are expected to scale as  $l^1$  for EE-orientated nanocubes.

**Computational details.** The PMFs and its energetic and entropic contributions are computed at distance increments of 0.2 nm for separations less than 2 nm from the distance of closest approach and 1 nm for larger separations. Since the nanocubes are composed of a rigid lattice of the silver atoms, tremendous computational savings can be achieved by simply pre-computing the vdW component of the total energy and forces. To further save computational costs, the interactions between the polymer beads and nanocube

lattice are pre-tabulated within a fine 3D Cartesian grid. The appropriate energy and force contributions from polymer-surface interactions can then be easily obtained via interpolation from grid values. To achieve ergodic sampling, we perform four independent simulation runs for each orientation and separation. Small deviations between the results computed from the four simulations suggested that the sampling was ergodic. The above quantities are computed for each of the FF and EE orientations and as function of varying chain lengths  $L$  (within the range 4–16 beads) and varying polymer-surface attraction strengths  $\epsilon_{ps}$  (within the range 0.02–0.08 kcal/mol). Note that the shortest chain length examined here interacts minimally with its neighbors on the same nanocube. Each simulation demanded between ~2–8 CPU hours on 2.2GHz AMD Istanbul processors. All other parameters, including the nanocube size, grafting density, force field, and temperature are fixed throughout the study.

**Table 1:** Parameter values describing our model for polymer-grafted nanocubes.

Parameter	Description	Value
$l$	Cube length	10 nm
$n_p$	Number of chains attached to each surface	4
$L$	Number of beads in each polymer chain	4–16
$l_0$	Equilibrium segment length of polymer	1 nm
$\theta_0$	Equilibrium angle between three chain beads	180°
$k_s$	Stretching constant of chains	10 kcal/mol/nm <sup>2</sup>
$k_\theta$	Bending constant of chains	0.1 kcal/mol/rad <sup>2</sup>
$\varepsilon_{pp}$	LJ energy parameter for polymer-polymer interactions	0.1 kcal/mol
$\varepsilon_{cp}$	LJ energy parameter for polymer-surface interactions	0.02–0.08 kcal/mol
$\varepsilon_{cc}$	LJ energy parameter for surface-surface interactions	1.23 kcal/mol
$\sigma_{pp}$	LJ size parameter for polymer-polymer interactions	1.0 nm
$\sigma_{cp}$	LJ size parameter for polymer-surface interactions	0.632 nm
$\sigma_{cc}$	LJ size parameter for surface-surface interactions	0.264 nm
$T$	Temperature	300 K

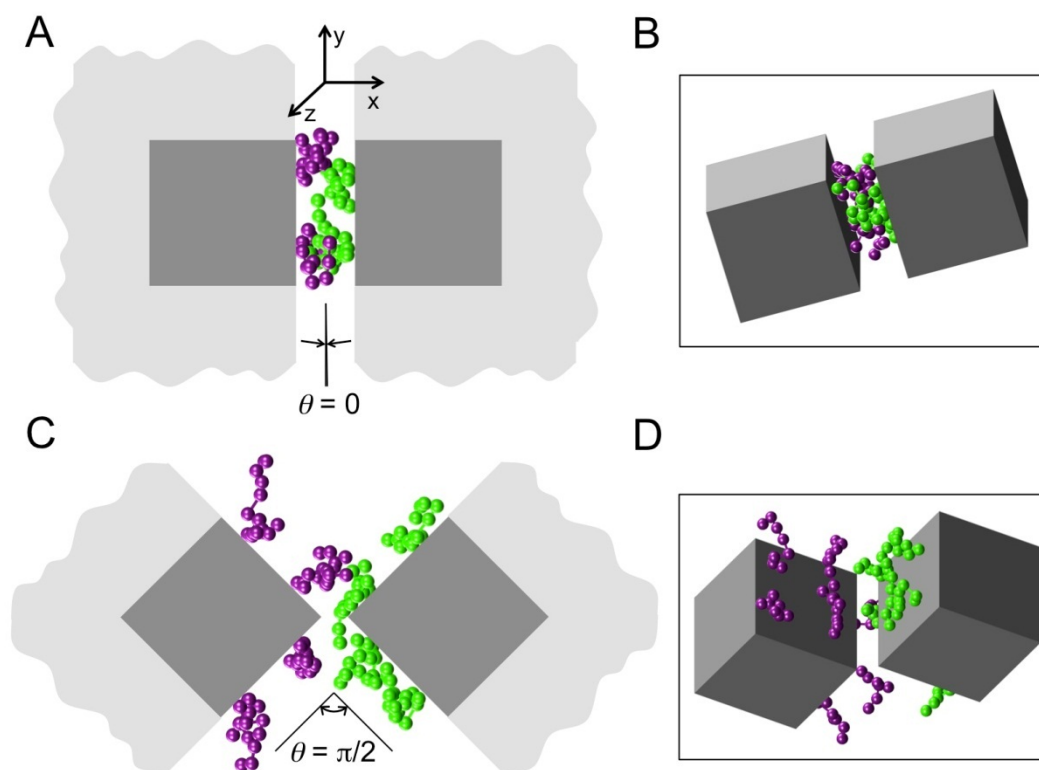


**Figure S3:** Coarse-grained model of polymer-grafted nanocubes employed to compute the PMF between nanocubes in the (A,B) FF and (C,D) EE configurations. We employ periodic boundary conditions (in the  $y$  and  $z$  directions for FF orientation and in the  $z$  direction for the EE orientation) to permit extrapolation of simulation results obtained for smaller 10-nm nanocubes (shown in dark grey) to the larger 80-nm nanocubes (shown only partially in light grey). Panels A and C show the top view and Panels B and D show isometric views.

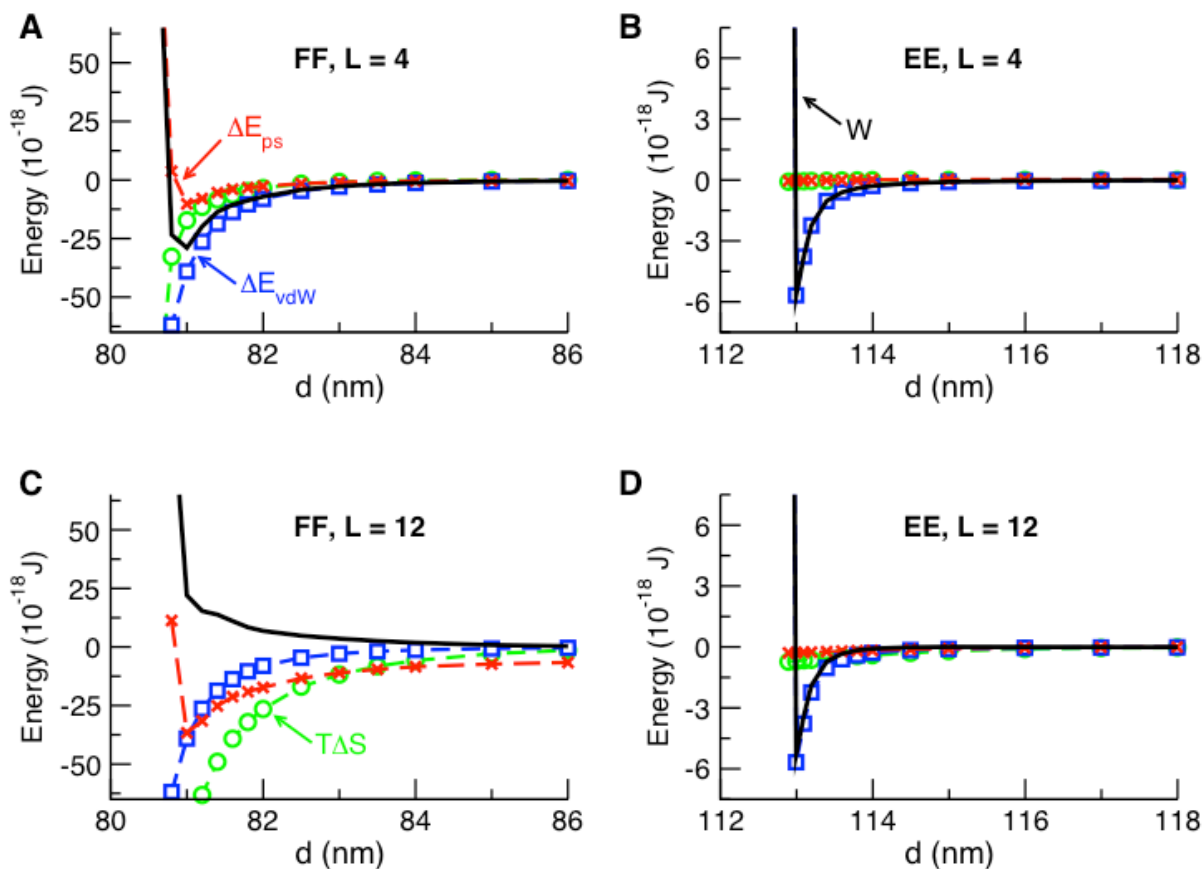


**Figure S4:** Contributions to PMF (solid black line) from steric repulsion between the grafted chains arising from loss in chain entropy  $T\Delta S$  (green circles), vdW attraction between the silver nanocubes  $E_{vdW}$  (blue squares), and the vdW plus excluded-volume interactions between the grafted chains and the nanocube surface  $E_{ps}$  (red crosses). Results are plotted for FF-oriented (A,C) and EE-oriented (B,D) nanocubes grafted with chains of lengths  $L = 4$  (A,B) and  $L = 12$  (C,D).

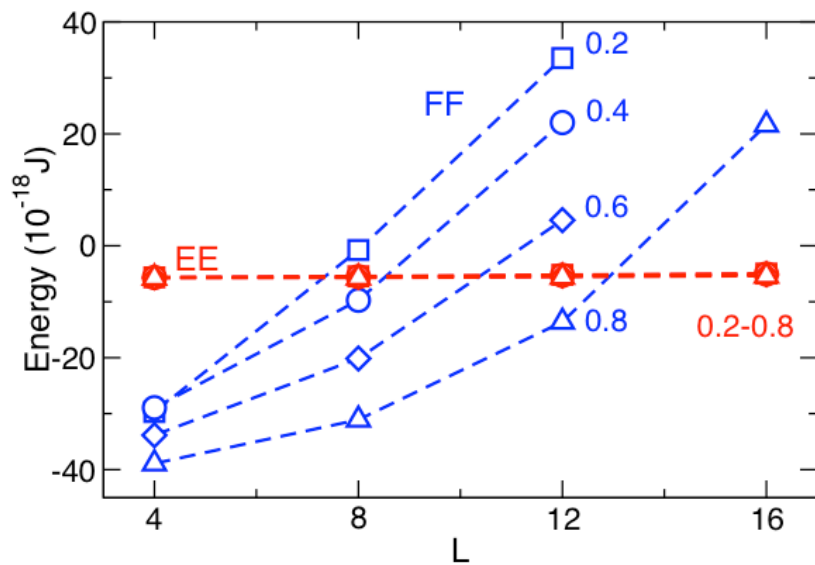


**Figure S5:** Attraction strength between polymer-grafted nanocubes, defined by the depth of the PMF minimum, as a function of chain length  $L$  for different polymer-surface interactions  $\epsilon_{ps}$ . Positive values correspond to repulsion and are taken to be the PMF at  $d = 81$  nm. Square, circle, diamond, and triangle symbols correspond to  $\epsilon_{ps} = 0.2, 0.4, 0.6,$  and  $0.8$ , respectively, and red and blue colors correspond to results for FF- and EE-oriented cubes, respectively.

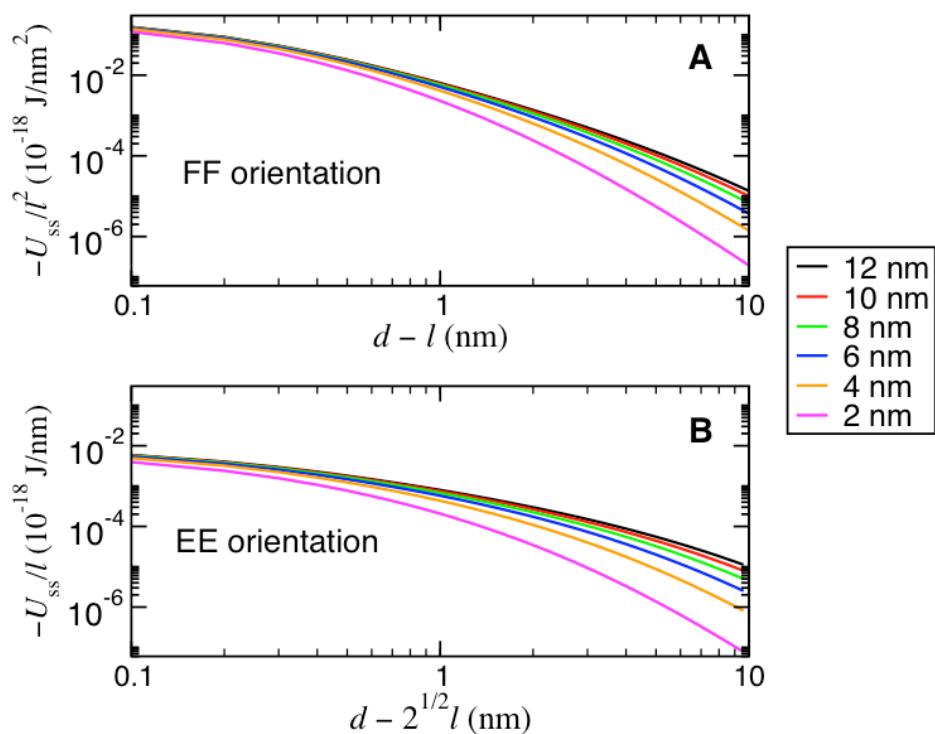


**Figure S6:** Normalized van der Waals energy  $\Delta U_{ss}$  computed for FF and EE-oriented nanocubes of sizes  $l$  in the range 2–12 nm as a function of gap distances.  $\Delta U_{ss}$  has been normalized by  $l^2$  for the FF orientation and by  $l$  for the EE orientation. That the normalized energy profiles converge for all particles, especially as the particles become larger and the gap distances smaller, confirms that the vdW energies scale as  $l^2$  and  $l$  for the FF and EE-oriented nanocubes, respectively.

#### 4. Surface Modification of the Nanocubes

For surface modification with PEG alkanethiol, PVP coated nanocubes deposited on PS film on substrate were incubated in a 2mM ethanol solution of (11-mercaptoundecyl)tetra(ethylene glycol) overnight at room temperature. The substrate was removed, followed by rinsing with copious ethanol to remove loosely bound PVP and thiol molecules and drying with N<sub>2</sub> before carrying out the solvent vapor anneal. Ideally, PVP on five out of the six faces of the nanocube (area fraction 0.83) is replaced by PEG alkanthiol. Nanocubes were modified with thiol terminated poly(N-vinylpyrrolidone) (Polymer source, 70% terminated with thiol group, M<sub>w</sub>=1700) using the same procedure. The ligand exchange process in each case was confirmed by infrared spectroscopy (Fig. S7). FTIR-ATR spectra taken of polymer-grafted nanocubes were recorded using a Nicolet System 6700 spectrometer with Smart-iTR. Spectra were recorded at 2 cm<sup>-1</sup> resolution and 128 scans were collected. After ligand exchange with PEG alkanethiol, the ATR-FTIR spectra of the resulted nanocubes were consistent with neat PEG alkanethiol: the appearance of a strong peak at 1130 cm<sup>-1</sup> corresponding to the C-O stretch; 1033 and 1056 cm<sup>-1</sup> vibrations (attributed to C-N stretching) and the carbonyl peak at 1662 cm<sup>-1</sup> from the initial PVP layer decrease in intensity, which suggest effective ligand exchange on nanocube surface. In the case of ligand exchange with thiol-terminated PVP, the ATR-FTIR spectra showed peaks at 693 and 770 cm<sup>-1</sup> attributed to the C-S stretch, and a strong carbonyl peak at 1676 cm<sup>-1</sup>. This suggests binding of PVP chains on the nanocube surface through a C-S moiety.

The FTIR spectrum associated with the as-made 55k PVP-coated nanoparticles is different than the shorter chain, PVP-thiol grafted nanocubes for two reasons. First, the 55k PVP is chemisorbed at the nanocube surface through interaction of Ag with the C=O groups of the pendant 2-pyrrolidone rings on the polymer chain. This strong binding interaction results in a large shift in the expected carbonyl peak position. Second, the nanocubes are synthesized at high solvent temperatures nearing 180-195°C. It is possible that upon adsorption to the Ag surface, a large number of carbon by-products are formed, as

evidenced by broad “carbon cathedral” peaks near  $1500\text{ cm}^{-1}$ . Such peaks are often indicative of carbon species that have “burned” at the metal surface, and are commonly observed during surface-enhanced Raman measurements of PVP-capped Ag surfaces. Upon incubation with thiol-terminated ligands, these by-products are likely displaced at the metal surface by formation of the metal-sulfur bond.

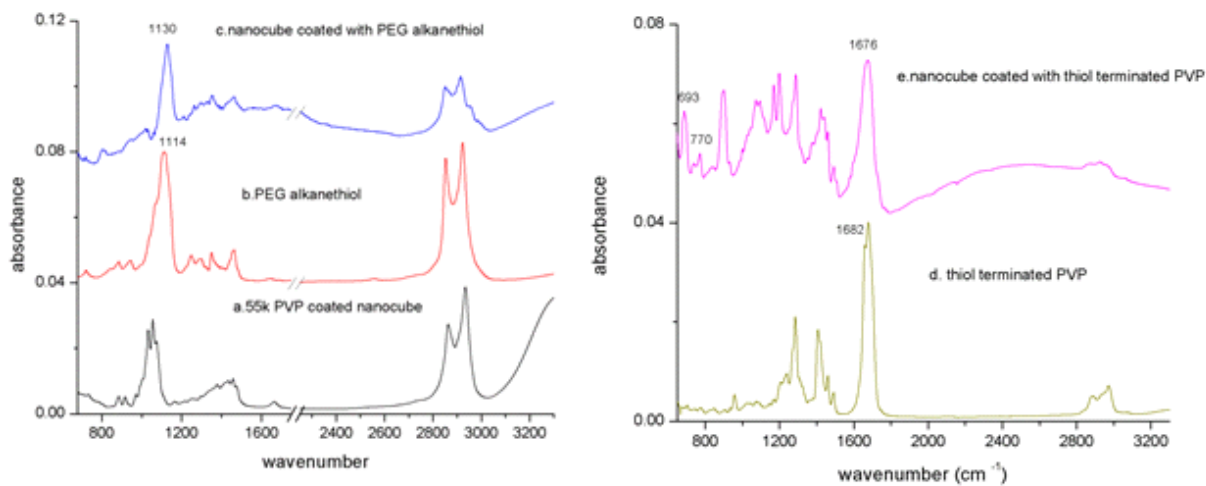


**Figure S7.** ATR-FTIR spectra of (a) as-made PVP coated nanocubes prior to ligand exchange, (b) neat PEG alkanethiol, (c) nanocubes after ligand exchange with PEG alkanethiol, (d) neat thiol-terminated PVP, (e) nanocubes after ligand exchange with thiol-terminated PVP. FTIR spectroscopy indicates that while ligand exchange is not 100% (as determined by monitoring the intensities of peaks associated with C-O and C=O bonds), incubation with PEG-thiol and PVP-thiol ligands does result in adequate ligand exchange to be considered “full coverage” of the nanoparticle surface.

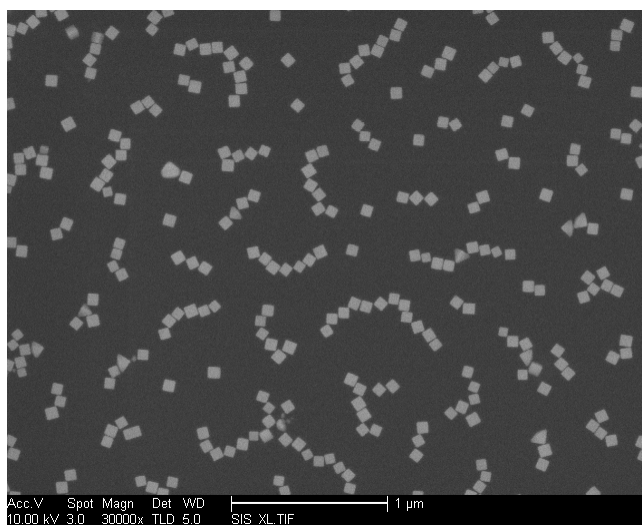


**Figure S8.** SEM of PEG-grafted nanocubes after 160 mins of solvent annealing, prior to thermal annealing. The nanojunctions adopt dominantly edge orientations, but the appearance of face orientations is significantly higher than for PVP-grafted nanocubes.

## 5. Nanocube String Length

Assembly statistics were obtained by considering the inter-NC orientation of the junction generated by two adjacent cubes. Samples were images using scanning electron microscopy and the orientations of the nanojunctions was considered over a  $50 \mu\text{m}^2$  film area. This resulted in the counting of approximately 1000-1200 cubes and between 700-1000 cube connections per sample, depending on the overall nanocrystal density within the polymer film.

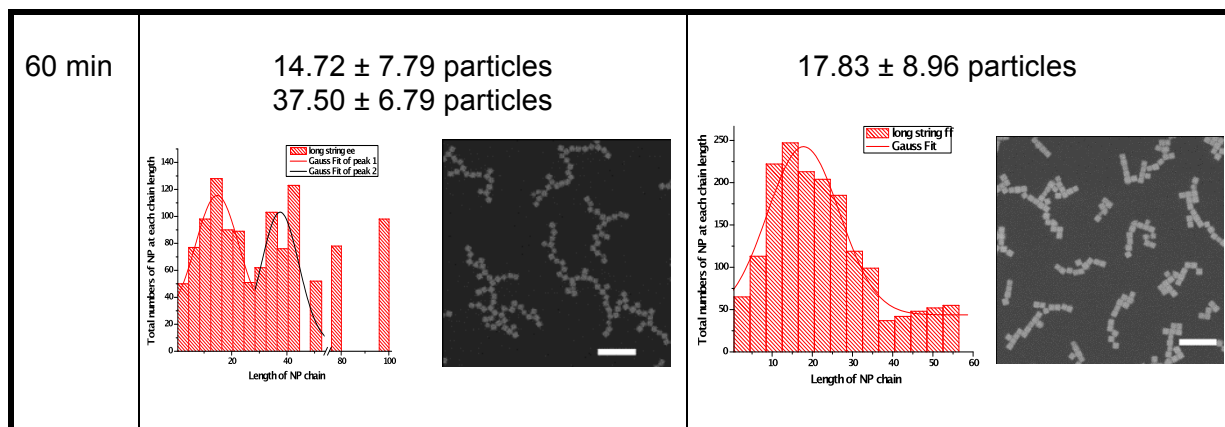
Nanojunction orientation of FF, EE, and FE configurations was determined by evaluating: i) angular orientation between adjacent cubes, ii) contact area between adjacent cubes, and iii) the distance from a cube corner to the center of the nanojunction. To distinguish between an EE- versus an FF-oriented structure, we consider the degree of electromagnetic coupling that occurs between adjacent nanocubes. In general, the degree of electromagnetic coupling between two adjacent metal surfaces is dependent on their separation distance. Based on our electrodynamic simulations, the separation distance between nanocubes must be smaller than 5 nm for significant electromagnetic coupling to occur. At a distance of 20 nm, electromagnetic coupling is too weak to facilitate hot spot formation. This is the criterion that we use to distinguish between EE and FF defects.

For an EE-oriented pair of nanocubes, the degree of coupling is dependent on the interparticle angle. Electromagnetic coupling is only facilitated between nanocube edges until a critical inter-cube angle of  $15^\circ$ . At this inter-cube angle, only  $< 20\%$  of the approaching cube faces are spaced less than 5 nm apart. The separation distance between the approaching nanocube edges (that do not comprise the EE nanojunction) is 20 nm. We use  $15^\circ$  as the inter-cube cut-off angle for an EE structure. For a FF-oriented pair of nanocubes, the degree of coupling is dependent on interaction area. Strong electromagnetic coupling is facilitated between FF-oriented nanocubes even when this interaction area is significantly decreased. We use a 50% interaction area as the cut-off for an FF defect.

The orientation statistics below were determined by counting nanojunctions for a sample set with the same approximate nanocube density. The images shown are representative of the overall assembly morphology across the entire sample area. Scale bar = 500 nm in the SEM images below.

**Table 2.** Nanocube counts for various string lengths. See footnote below.\*

Time	EE-oriented	FF-oriented
15 min	<p><math>1.24 \pm 0.48</math> particles</p>	<p><math>1.01 \pm 0.45</math> particles</p>
30 min	<p><math>1.78 \pm 1.02</math> particles</p>	<p><math>2.40 \pm 1.54</math> particles</p>
45 min	<p><math>5.70 \pm 2.50</math> particles</p>	<p><math>6.57 \pm 4.12</math> particles</p>



\*The EE oriented cubes are obtained using PVP-grafted particles. The FF oriented cubes are obtained using PEG-grafted particles. The PEG-grafted samples are first exposed to chloroform vapor to form EE assemblies with a desired string length before carrying out thermal annealing for 4 hours at 120°C.

## 6. FEM Simulations

The finite element method was used to calculate the scattering spectra and electric field distributions for Ag nanocubes. We used a commercially available software package (COMSOL v 4.2a with the RF module) to numerically solve for near- and far-field optical properties of the nanocubes in the frequency domain using the scattered field formulation. The 3D simulation space was composed of two spherical volumes - the embedding medium and a perfectly matched layer (PML) – and the nanocube structures under investigation. Bulk dielectric constants were obtained from Johnson and Christy [13] with linear interpolation. Nanocubes were modeled to match experimental conditions, with edge lengths = 80 nm and separation gaps of 2 nm. An unpolarized plane wave, used for excitation, was inserted on the inside of the PML surrounding the embedding medium. Discretization of the simulation space was conducted using the built-in free meshing algorithm in COMSOL, which partitioned the simulation space into a collection of tetrahedral finite elements. Scattering spectra were calculated on a spherical boundary using the COMSOL implementation of the Stratton-Chu formula with incident electric field strength of  $E_o = 1$  V/m. Field intensities depicted in each field distribution plot are in units of V/m. The electromagnetic field enhancement factor ( $EF$ ) is calculated by taking  $EF = E / E_o$ .

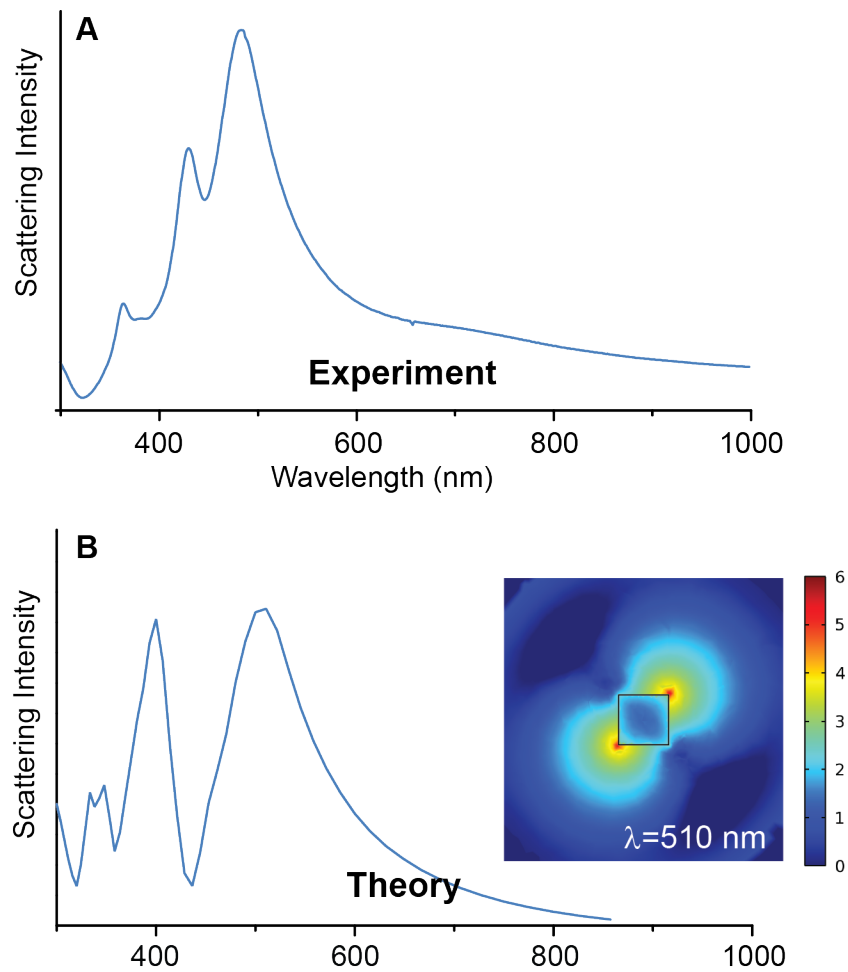


**Figure S9.** Left: Optical scattering of isolated nanocubes distributed within a polystyrene film, prior to assembly. Right: Theoretical far-field response of a single cube with edge length = 80 nm. Inset: Electric field distribution (color, log (2) scale) for excitation of the dipolar localized surface plasmon resonance. For a cube centered at the origin, the inset shows a two-dimensional slice that corresponds to field strength in the x-y plane of the cube.

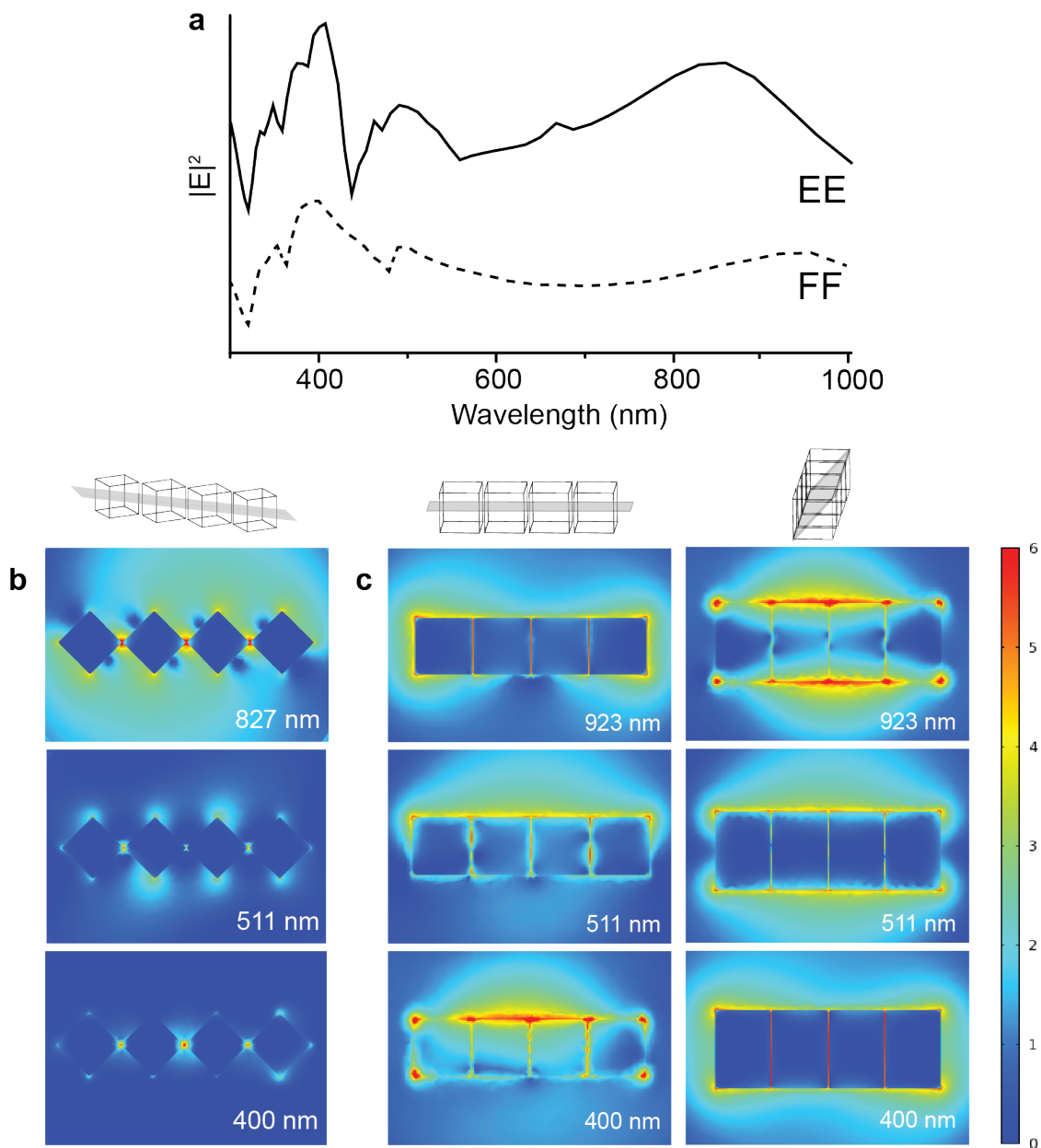


**Figure S10.** (a) The calculated far-field scattering spectrum for a string of four nanoparticles aligned in EE (solid) and FF (dotted) configurations. (b,c) The calculated electric field strengths (color) at various SP wavelengths for the nanoparticle strings modeled in part (a). For cube assemblies centered at the x-y plane, the field distributions are depicted for a two-dimensional slice at (b) the x-y plane and (c) both the

x-y plane and the plane along the cube diagonal, as shown. For visual contrast, the electric potential is plotted using a log (2) scale with min/max cutoffs as shown.

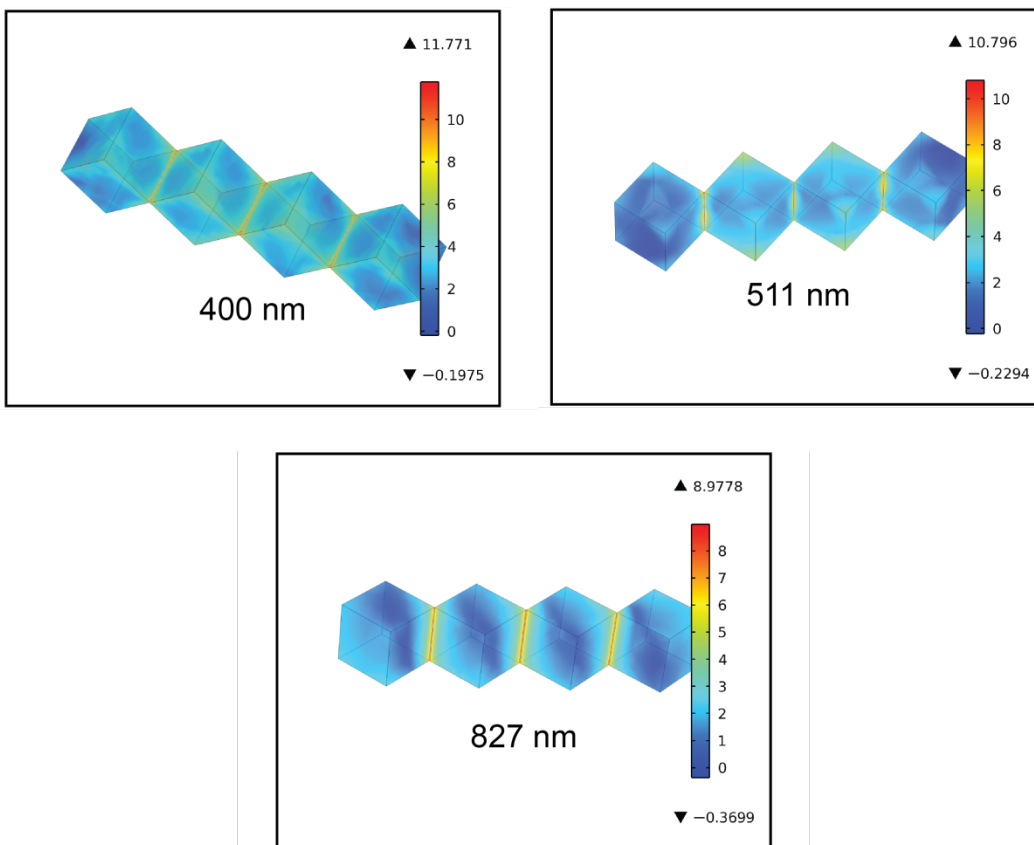


**Figure S11.** Plot of the calculated electric field strength for nanoparticle strings oriented in the EE configuration. For visual contrast, the electric potential is plotted using a log (2) scale with min/max cutoffs as shown.

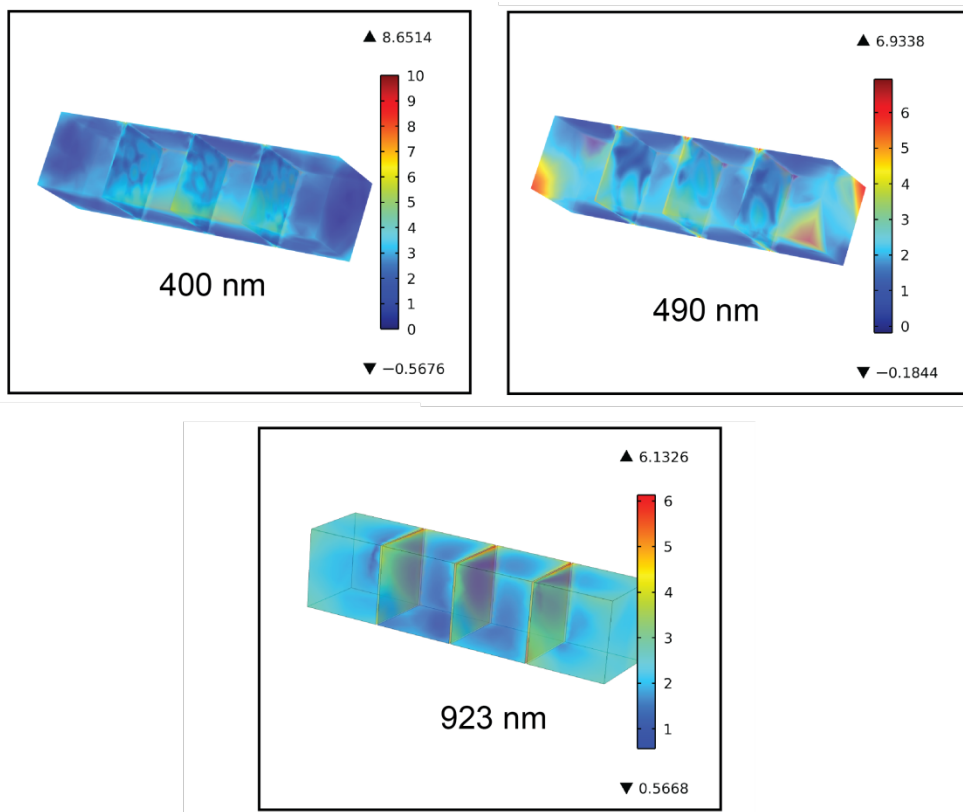


**Figure S12.** Plot of the calculated electric field strength for nanoparticle strings oriented in the FF configuration. For visual contrast, the electric potential is plotted using a log (2) scale with min/max cutoffs as shown.

## 7. Additional Experiments with Long-Chain PEG Grafts

To confirm that the transition from EE-oriented nanocubes to FF-oriented nanocubes is dependent on polymer graft chain length and not specific chemical interactions, we carried out additional experiments follow the assembly of nanocubes modified with long PEG grafts with  $M_w = 5k$  (Laysan Bio, Inc.) and  $M_w = 54k$  (Polymer Source).

Figure S13 shows the results of experiments carried out with long PEG grafts with  $M_w = 54k$ . These films show a large number of EE orientations, but result in nanocube assemblies that also contain a large number of assembly defects. This is due to artifacts associated with polystyrene dewetting from the nanocube surface. We have observed that PEG-thiols with longer PEG chains do not carry out complete displacement of the ligands present on the silver surface. This is confirmed by FTIR, which shows the presence of both C-O bonds (from PEG) and C=O bonds (from PVP, which is present on the as-synthesized nanocubes). Recently published work suggests that PEG grafts with  $M_w > 20k$  lose their random coil configuration and adopt globule-like conformations when attached to a nanoparticle surface. Poor surface modification with PEG is likely to explain the observed matrix dewetting.

In contrast, PEG grafts with  $M_w = 5k$  are expected to remain in a brush-like configuration when attached to a nanoparticle surface. Figure S14 shows SEM images of the same nanocube film after (a) surface modification with the 5k PEG graft, (b) followed by 160 minutes of solvent annealing under chloroform vapor, and (c) followed by 4 hours of thermal treatment at 120° C. After solvent treatment, the nanocubes assemble into predominantly EE-oriented strings. Out of a total of 345 nanojunctions, we counted  $13.4 \pm 2.6\%$  face orientations,  $75.2 \pm 1.9\%$  edge orientations, and  $11.4 \pm 3.0\%$  uncategorized orientation defects. Defects resulting from dewetting of the matrix polymer are still present (some examples circled in red), although significantly minimized in comparison to longer PEG grafts. After thermal annealing, we observe that the previously dewetted matrix polymer is redistributed around the nanocubes and that the nanocubes remain assembled in the EE-orientation. Out of a total of 356

nanojunctions, we counted  $15.8 \pm 2.1\%$  face orientations,  $77.1 \pm 2.1\%$  edge orientations, and  $7.1 \pm 0.9\%$  uncategorized orientation defects. Thus, we do not observe significant conversion to the FF orientation.

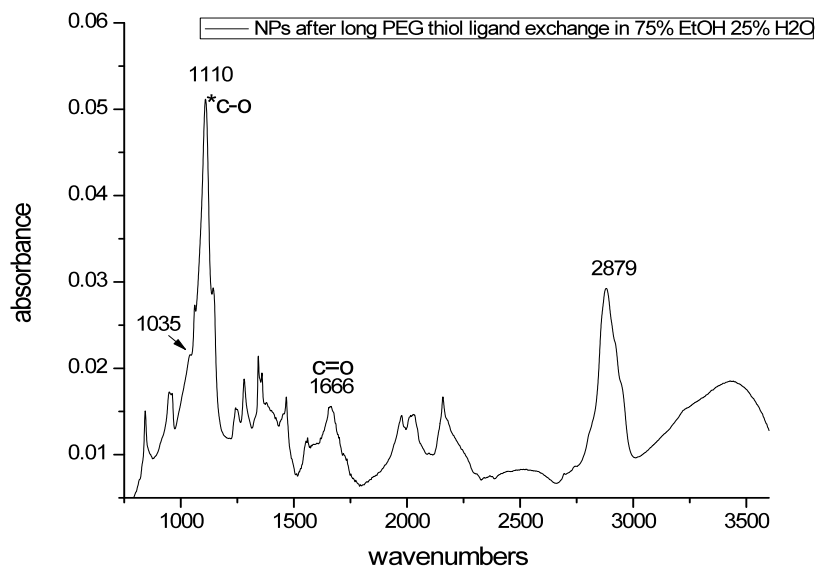
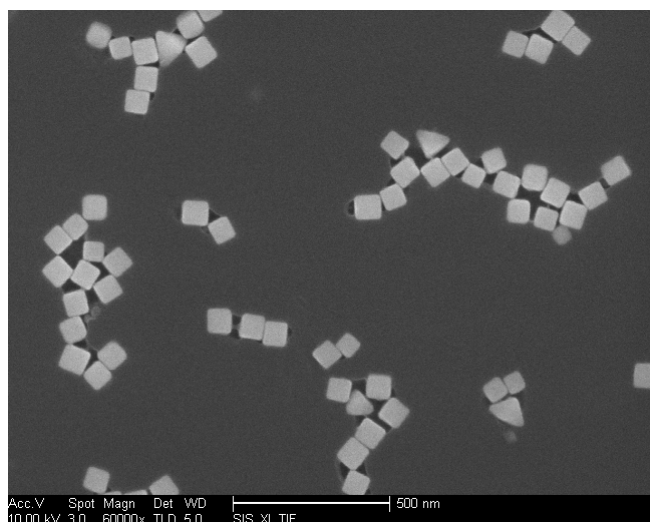
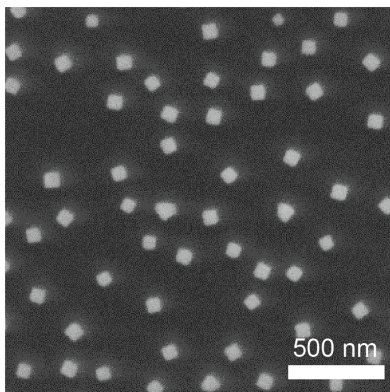
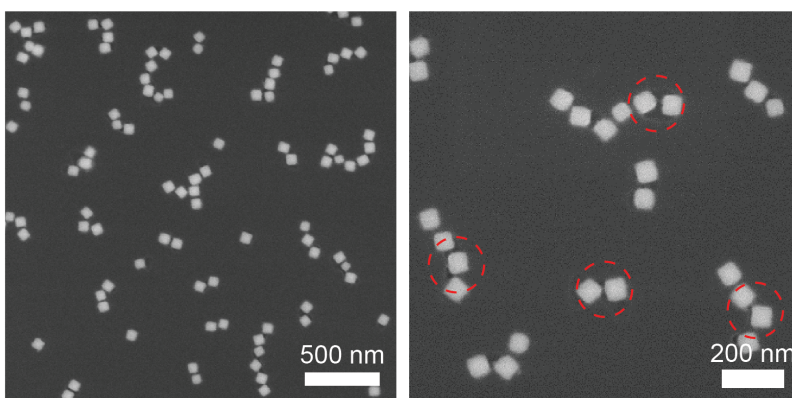


**Figure S13.** A representative SEM image of nanocube assemblies generated with nanocubes grafted with long PEG-thiol chains ( $M_w = 54k$ ) and an FTIR spectrum of similarly modified nanocubes.

(a) After surface modification with PEG-thiol ( $M_w = 5k$ )



(b) After 160 minutes of exposure to chloroform vapor



(c) After 4 hours of thermal treatment at 120° C.

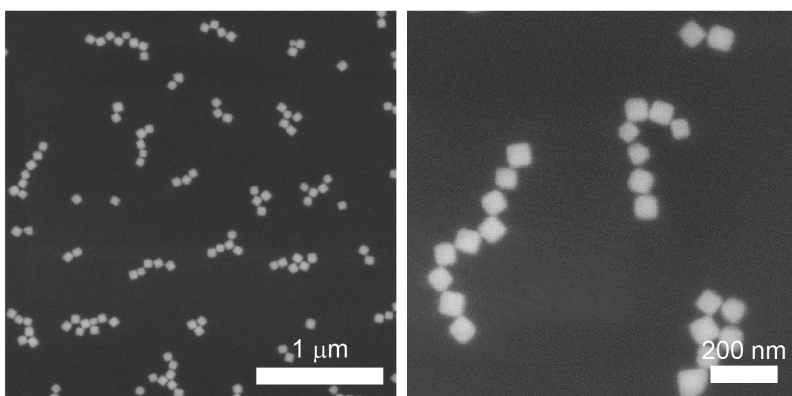


**Figure S14.** SEM images of the same nanocube film obtained by modifying nanocubes with PEG-thiol grafts of  $M_w = 5k$ . Images show the nanocubes after (a) surface modification with the PEG graft, (b) followed by 160 minutes of solvent annealing under chloroform vapor, and (c) followed by 4 hours of

thermal treatment at 120° C. Red dashed circles indicate areas of matrix polymer dewetting.

## References

1. Y. Sun, Y. Xia, *Science* 298, 2176 (2002).
2. A. Tao, P. Sinsersuksakul, P. Yang, *Angewandte Chemie International Edition* 45, 4597 (2006).
3. Arya, G. *J. Phys. Chem. B* 2009, 113, 15760–15770.
4. Arya, G. *J. Phys. Chem. B* 2010, 114, 15886–15896.
5. Israelachvili, J. *Intermolecular & Surface Forces*; Academic Press: London, 1991.
6. Eichenlaub, S.; Chan, C.; Beaudoin, S. P. *J. Colloid Interface Sci.* 2002, 248, 389-397
7. McQuarrie, D. A. *Statistical Mechanics*; University Science Books: Sausalito, California, 2000.
8. Siepman, J. I.; Frenkel, D. *Mol. Phys.* 1992, 75, 59–70.
9. Frenkel, D.; Mooij, G. C. A. M.; Smit, B. *J. Phys.: Cond. Matter.* 1992, 4, 3053–3076.
10. de Pablo, J. J.; Laso, M.; Suter, U. W. *J. Chem. Phys.* 1992, 96, 2395–2403.
11. de Rocco, A. G.; Hoover, W. G. *Proc. Natl. Acad. Sci.* 1960, 46, 1058-1065.
12. Langbein, D. *Theory of Van der Waals attraction*, in Springer Tracts in Modern Physics; Springer: Berlin, 1974.
13. Johnson, P. B.; Christy, R. W. *Physical Review B.* 1972, 6, (12), 4370.
14. X. Xia, M. Yang, Y. Wang, Y. Zheng, Q. Li, J. Chen and Y. Xia. *ACS Nano* 2012, 6 (1), 512–522.